Asian Journal of Chemistry; Vol. 32, No. 2 (2020), 297-302

ASIAN JOURNAL OF CHEMISTRY

https://doi.org/10.14233/ajchem.2020.22321

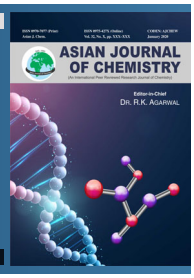

Synthesis, Characterization and Anticancer Activity of Transition Metal Substituted Polyoxometalate-β-Cyclodextrin Composites

BHARATH SAMANNAN, JOTHI SELVAM and JEYABALAN THAVASIKANI*

Department of Chemistry, Sacred Heart College, Tirupattur-635601, India

*Corresponding author: E-mail: jayabalandr@gmail.com

Received: 10 July 2019; *Accepted*: 12 September 2019; *Published online*: 30 December 2019; AJC-19716

A novel hybrid composite, namely {[$V^{IV+}PMo_{11}O_{40}$]⊂[β-CD]} which shows the high percent of apoptosis of MTT assay of A549 cell line (lung cancer) in different concentrations. The composite has been characterized using techniques such as FT-IR, EPR, SEM, EDS and X-ray diffraction. The anticancer (lung cancer A549 cell line) was investigated using direct microscopic observations for drug treated cell line and IC_{50} value of 1.93. The apoptosis of 45.37 % cell death in cell line of minimum concentration (3.12 μg/mL) shows the good viability of β-CD-POM against lung cancer A549 cell line.

Keywords: Anticancer, β-Cyclodextrin, Hybrid composite, Polyoxometalate.

INTRODUCTION

In today's World, cancer become serious problem which threaten human health. Heteropolyacid has effective role in the field of antitumor, anticancer likely breast cancer, lung cancer and so on [1]. The host-guest molecules are promising composite of hybrid system in last few decades of chemistry [2].

Polyoxometalate (POM) is a molecular inorganic quasi semiconductor has electroconductive and electron acceptor properties which have been reported previously [3]. The hybrid system like keggin type polyoxometalate has been used for sensor application [4]. Polyoxometalateis a metal-oxygen cluster doped organic material has been exhibiting antitumor and anticancer activity [5], electronic properties, photo-catalytic activity [6] and energy storage [7]. Polyoxometalate has contained W or Mo atoms in their highest oxidation state which results in supercapacitive energy storage [8]. The interchangeable of X central metal atom site like V^{5+}, Mn^{4+} and Fe^{3+} has used for ion battery anodes and conductive properties [9]. This compounds have used more frequently than unsubstituted material. For example, the presence of metal M in the bony structure of [$NH_{4-n}PMo_{12-n}O_{40}$] to [$NH_{4+n}V_nPMo_{12-n}$] a particular temperature, pH, assemble into monomeric species [10].

Cyclodextrin (CD) a bio-polymer is the important compound which is effective in host-guest inclusion complex [11]. Most of the guest molecules are suitable in the cavity of β-CD. Interlayer hydrophilic and outer layer hydrophobic cavities toroidal molecules which allow encapsulation of acceptable guest compound [12]. β-Cyclodextrin has conjugated with polyoxometalate by replacing conductive polymer with various applications [13]. β-Cyclodextrin have low water-soluble among CDs, they have been most applied field is drug delivery due to its host-guest aptitude. The host-guest complex involving an α-cyclodextrin and dawson type POM hybrid has been previously reported in the literature [14]. The formation of the hybrid system and their properties such as potential has led to applications into various fields like Anticancer, nanotechnology and environmental science [15-18].

Organic-inorganic interactions between POM-β-cyclodextrin composite are effective field in chemistry [19]. Polyoxometalate guest molecule which has exchanged interlayer anion into a positive charge of atomic distribution of metal cations with cyclodextrin for catalytic application has been reported in the literature [20]. In the earlier report, organic-inorganic hybrid system of Dawson type POM conjugated α-cyclodextrin [21]; we have tried to conjugate Keggin type POM in β-cyclodextrin outer cavity to study on conductivity

of inclusion composite. The organic-inorganic hybrid system of β-cyclodextrin conjugated POM exhibits the higher apoptosis by using direct microscopic observations for drug treated cell line and IC_{50} value of 1.93. In this paper, synthesis, characterization and anticancer activity of transition metal substituted polyoxometalate-β-cyclodextrin composites has been discussed.

EXPERIMENTAL

All chemicals reagents like ammonium metavanadate, ammonium molybdate, disodium hydrogen phosphate, conc. HNO_3 were purchased from Merck and β-cyclodextrin were purchased from Sigma Aldrich.

Preparation of the polyoxometalate: Polyoxometalate is prepared by mixing a solution of ammonium metavanadate (0.5 g) in 10 mL of H_2O and ammonium molybdate (2 g) in 10 mL of H_2O (white to purple colour) with continues stirring. To this hot solution, aqueous solution of disodium hydrogen phosphate (0.5 g) in 10 mL of H_2O and few drops conc. HNO_3 was added with continuous stirring for next 1 h. The solution was cooled, filtered and dried at room temperature. (I) calculated by gravimetric analysis: Mo - 66.46 %, V - 2.94 %. (II) In EDS results show that the presence of oxygen is O – ± 36.30 %, Mo - 66.27 % and V - 2.90 %.

Preparation of the complex (II): Complex (II) was prepared by adapting a similar procedure used for the preparation of polyoxometalate. In this hot solution, (0.009 M) of β-cyclodextrin is added with constant stirring for another 2 h. The orange colour powder obtained from the solution upon ageing for next 3 days. The formed powder was filtered, washes with ethanol and dried at room temperature. (I) calculated by gravimetric analysis: Mo – 38.13 % and V – 1.60 %. (II) In EDS result shows that the presence of oxygen is O – ± 41.05 %, Mo – 38.39 %, V – 1.69 % and C -19.44 %.

Analytical and physical methods: FT-IR was carried out using a spectrometer SHIMAZDU FT-IR using the KBr pellets. The morphological structure of complex was investigated using SEM (JOEL JSM 6390). X-ray diffraction were collected using SHIMAZDU XRD-6000, operating in Bragg-Brentano focusing geometry and using Cu Kα radiation (λ = 1.5418 Å) from a generator operating at 40 kV and 30 mA. The conductivity measured by alternating current (AC) impedance analyzer in the range of 273-298 K, exhibiting a maximum value of 10^{-7} S cm^{-1} at 298 K for organic-inorganic complexes. JEOL Model JES FA200 instrument is the state of the art electron spin resonance (ESR) spectrometer used for the measurement of species that contain unpaired electrons (free radicals, transition metal complexes, odd-electron molecules, rare earth ions *etc*.) X-Band frequency: 8.75-9.65 GHz, Sensitivity: 7×10^9 spins/0.1 mT, Resolution: 2.35 μT or better variable temperature facility (-153 to +25 °C).

RESULTS AND DISCUSSION

Cell culture: A549 (Lung cancer) cell lines were procured from NCCS, stock cells was cultured in medium supplemented with 10 % inactivated fetal bovine serum (FBS), penicillin (100 IU/mL), streptomycin (100 μg/mL) in an humidified atmosphere of 5 % CO_2 at 37 °C until confluent. The cell was dissociated with TPVG solution (0.2 % trypsin, 0.02 % EDTA, 0.05 % glucose in PBS). The viability of the cells are checked and centrifuged. Further 50,000 cells/well was seeded in a 96 well plate and incubated for 24 h at 37 °C, 5 % CO_2 incubator.

Cytotoxicity studies

MTT assay: The *in vitro* determinations of toxic effects of unknown compounds have been performed by counting viable cells after staining with a vital dye. Alternative methods used are measurement of radioisotope incorporation as a measure of DNA synthesis, counting by automated counters and others which rely on dyes and cellular activity. The MTT system is a means of measuring the activity of living cells *via* mitochondrial dehydrogenases. The MTT method is simple, accurate and yields reproducible results. The key component is (3-[4,5-dimethylthiazol-2-yl]-2,5-diphenyltetrazolium bromide) or MTT, is a water soluble tetrazolium salt yielding a yellowish solution when prepared in media or salt solutions lacking phenol red. Dissolved MTT is converted to an insoluble purple formazan by cleavage of the tetrazolium ring by mitochondrial dehydrogenase enzymes of viable cells. This water insoluble formazan can be solubilized using DMSO, acidified isopropanol or other solvents (pure propanol or ethanol). The resulting purple solution is measured spectrophotometrically. An increase or decrease in cell number results in a concomitant change in the amount of formazan formed, indicating the degree of cytotoxicity caused by the test material.

Procedure: The monolayer cell culture was trypsinized and the cell count was adjusted to 1.0×10^5 cells/mL using respective media containing 10 % FBS. To each well of the 96 well microtiter plate, 100 μL of the diluted cell suspension (50,000 cells/well) was added. After 24 h, when a partial monolayer was formed, the supernatant was flicked off, washed the monolayer once with medium and 100 μL of different test concentrations of test drugs were added on to the partial monolayer in microtiter plates. The plates were then incubated at 37 °C for 48 h in 5 % CO_2 atmosphere. After incubation the test solutions in the wells were discarded and 100 μL of MTT (5 mg/10 mL of MTT in PBS) was added to each well. The plates were incubated for 4 h at 37 °C in 5 % CO_2 atmosphere. The supernatant was removed and 100 μL of DMSO was added and the plates were gently shaken to solubilize the formed formazan. The absorbance was measured using a micro plate reader at a wavelength of 570 nm. The percentage growth inhibition was calculated using the following formula and concentration of test drug needed to inhibit cell growth by 50 % (IC_{50}) values is generated from the dose-response curves for each cell line.

IC_{50} value: The half maximal inhibitory concentration (IC_{50}) is a measure of the effectiveness of a compound in inhibiting biological or biochemical function. This quantitative measure indicates how much of a particular drug or other substance (inhibitor) is needed to inhibit a given biological process (or component of a process, *i.e.* an enzyme, cell, cell receptor or microorganism) by half.

The IC_{50} of a drug can be determined by constructing a dose-response curve and examining the effect of different concentrations of antagonist on reversing agonist activity. IC_{50} values can be calculated for a given antagonist by determining the

concentration needed to inhibit half of the maximum biological response of the agonist. IC_{50} values for cytotoxicity tests were derived from a nonlinear regression analysis (curve fit) based on sigmoid dose response curve. The direct microscopic observations of drug treated images of cell line by inverted biological microscope was enclosed with the report.

FT-IR: FT-IR spectra show the change in frequency of functional groups of β-CD-POM than that of the pure POM, β-cyclodextrin after the formation of the complex (β-CD-POM). Fig. 1 shows IR spectra of POM, β-CD and β-CD-POM and their tentative assignments are given in Table-1. The guest molecule (POM) shows bands at 1059, 1020, 938 and 820 cm^{-1} is corresponding to the stretching frequency of P-O, M-O_b inter, M-O_b (intra) and M-O-M (M = V^{IV}), respectively. The stretching vibrations at 1632 and 3432 cm^{-1} is assigned to ν(OH) symmetric or H-bonded in a different way. The band at 894 cm^{-1} shows the presence of β-(1,4)-glucopyranose ring of β-CD is an important tentative assignment. This band frequency shows the presence of the conjugated complex. The two bands at 1030 and 1160 cm^{-1} indicates the ν(C-O-C) stretching vibrations. One at 1400 cm^{-1} is assigned to ν(O-CH) and ν(C-H) bonds. A one at 2930 cm^{-1} is corresponding to the ν(CH_2) stretching vibration. The stretching vibration at (1645→1624) cm^{-1} and (3350 →3414) cm^{-1} in the IR spectra is assigned to δ(HOH) of two different types of water molecule existing in the cavities of β-CD-POM. In pure β-CD band at 3350 cm^{-1} shows broad water molecules group whereas the inclusion complex found to be narrowed in the FT-IR spectrum (3414 cm^{-1}) which is a good indication of the formation of inclusion complex as previously reported [22]. The upward shift at (1059→1074), (938→976) cm^{-1} indicates the tentative assignments of P-O, M-Ob inter. One at 1020 cm^{-1} in POM is absence in β-CD-POM is may be due to the interaction of host-guest complex. The quenching or downward shift at 805 cm^{-1} indicates the M-O-M (M = V^{IV}, Mn^{IV}) stretching vibration. The band at 897 cm^{-1} with a minor increase in the frequencies is due to the β-(1,4)-glucopyranose ring of β-CD inclusion with POM. One at 1029 and 1174 cm^{-1} is corresponding to the stretching frequency of ν(C-O-C) bonds. The upward shift of ν(CH_2) bond is observed at 2932 and 1477 cm^{-1} indicates the presence of ν(O-CH) and ν(CH) stretching. Table-1 shows some increase and decreases in the intensity changes (Δδ). The band frequencies increase may be due to the oxo-metal group into the electron-rich outer cavity of β-CD

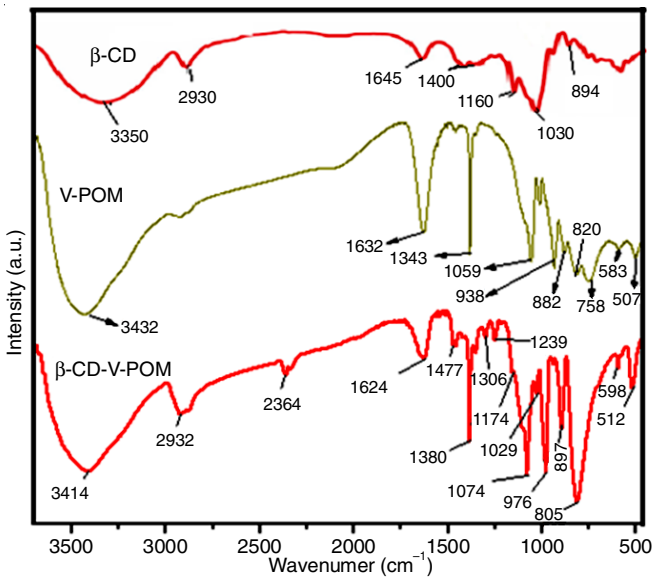

Fig. 1. IR spectra of POM, β-CD and β-CD-POM as KBr disks

which enhances the density of electron cloud in the inclusion complex [23]. The formation of hydrogen bonding and van der Waals forces interacts to form an inclusion complex. This lead to a decrease in the frequency between the inclusion complex and its guest molecule (POM) is due to the changes in the microenvironment [24].

X-ray diffraction: XRD spectra of the complex β-CD-POM along with the pure β-CD and POM are shown in Fig. 2. The grain size, crystallinity and spectral data are given in Table-2. The POM exhibits peaks at 7.9, 9.1, 21, 27.5 and 35.4 are corresponding to the (JCPDS Card No. 87-0546). The peak at 21 and 27 is assigned to the presence of the vanadium in the prepared POM (JCPDS 41-1426). The pure β-CD shows peak at 9, 12.5, 18.1 and 47 observed to the (JCPDS Card No. 32-1626 and 27). The bands at 7.8, 9.8, 18.67 and 22.86 were corresponding to the β-CD-POM inclusion complex. There is no much amphorous site in the complex β-CD-POM. Due to the host-guest interactions, whereas the host molecule (β-CD) interacts with a guest molecule (POM) causes an increase in the grain size of the complex compared to POM and β-CD. Presence of the reflection of POM and β-CD in XRD patterns of β-CD-POM complex attests the successful formation of a complex structure of this compound.

TABLE-1
IR SPECTRAL DATA OF POM, β-CD AND β-CD-POM

Ligand (guest) $[XMo_{12}O_{40}]^{n-}$ (X = V^{IV})	Ligand (host) β-CD	Complexes β-CD-POM	Band assignments	Reference	Changes Δδ
1059	–	1074	P-O	1100-1070 [Ref. 25]	+15
1020	–	1029	M-O_b intra	1050-990 [Ref. 25]	+9
938	–	976	M-O_b inter	976-930 [Ref. 25]	+38
820	–	805	M-O-M (M = V^{IV}, Mn^{IV})	800 [Ref. 25]	-15
–	894	897	β-(1,4)-Glycopyranose ring		+3
–	1030	1029	ν(C-O-C)	1027 [Ref. 26]	-1
–	1160	1174	ν(C-O-C)	1158 [Ref. 26]	+14
1632	1645	1624	ν(HOH)	1650 [Ref. 27]	-19
–	2930	2932	ν(CH_2)	2925 [Ref. 26]	+2
–	1400	1477	ν(O-CH], ν(CCH)	1420 [Ref. 27]	+77
3432	3350	3414	ν(OH) symmetric	3389 [Ref. 26]	+64

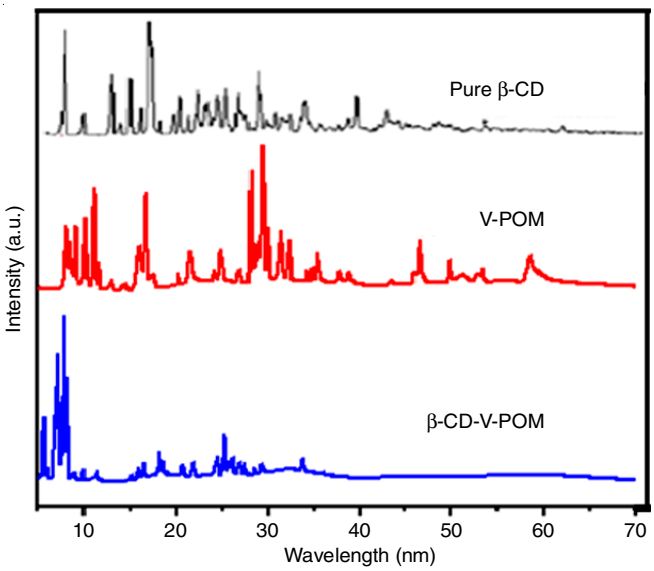

Fig. 2. XRD pattern of POM, β-CD and β-CD-POM

TABLE-2
XRD SPECTRAL DATA OF POM, β-CD AND β-CD-POM

Samples	2θ value	Grain size (nm)
POM	7.9	26
	9.1	35
	21.0	29
	27.5	25
	35.4	27
β-Cyclodextrin	9.0	30
	12.5	28
	18.1	27
	47.0	34
β-CD-POM	9.80	48
	12.90	37
	18.67	35
	22.86	23

Morphology study: Fig. 3a shows the SEM image of POM, where nanoparticle exhibits like microflower form and smaller size than β-CD-POM inclusion complex. The SEM images display the particles are agglomerated and unevenly distributed to form a flower-like shape. The average particle size of the POM sample is 5 μm. The structure of the complex β-CD-POM is shown in Fig. 3b. The images obtained for the complex β-CD-POM sample presents the existence of like rectangular shape block, opaque structure. The nanoparticles of POM covered on its surface with grains of size similar that are evenly self-assembled. The geometry of oxo-metal groups β-CD-POM complex form into a self-assembled structure with size 630 nm.

X-Band EPR studies: The electrons are negatively charged particle which acquires orbital angular momentum and estimates around the core (nuclei). The EPR spectra (Fig. 4) give resonances typical V^{IV}. The sharp peak indicates at (magnetic field 3400 mT and frequency 9.45 MHz) vanadium(IV) in POM .

The X-band EPR spectroscopic studies for POM and β-CD-POM reveals hyperfine structure show (V^{+}) in the 8 hyperfine lines of EPR spectral signals. The calculated EPR spectral g value of POM and β-CD-POM is 1.90 and 1.98 given in Table-3. Due to the charge (electron) transfer causes the activation of M-O-M bonding. Initially, Mo^{V}/Mo^{IV} moderate process give vanadium doped POM. Its unsubstituted linearly depends on their total charge of the electron and bond valance. The imitative from the bond length indicates the formation of the oxygen is bonded to a heteroatom. These show that a nucleus is the close vicinity of the reduced V^{IV} atom attached along with POM and identified as hyperfine couplings. Structural electron polarizability from the quenching of the guest molecules occurs due to the interaction with the frozen localized electron density of the polar carbon host molecule [28].

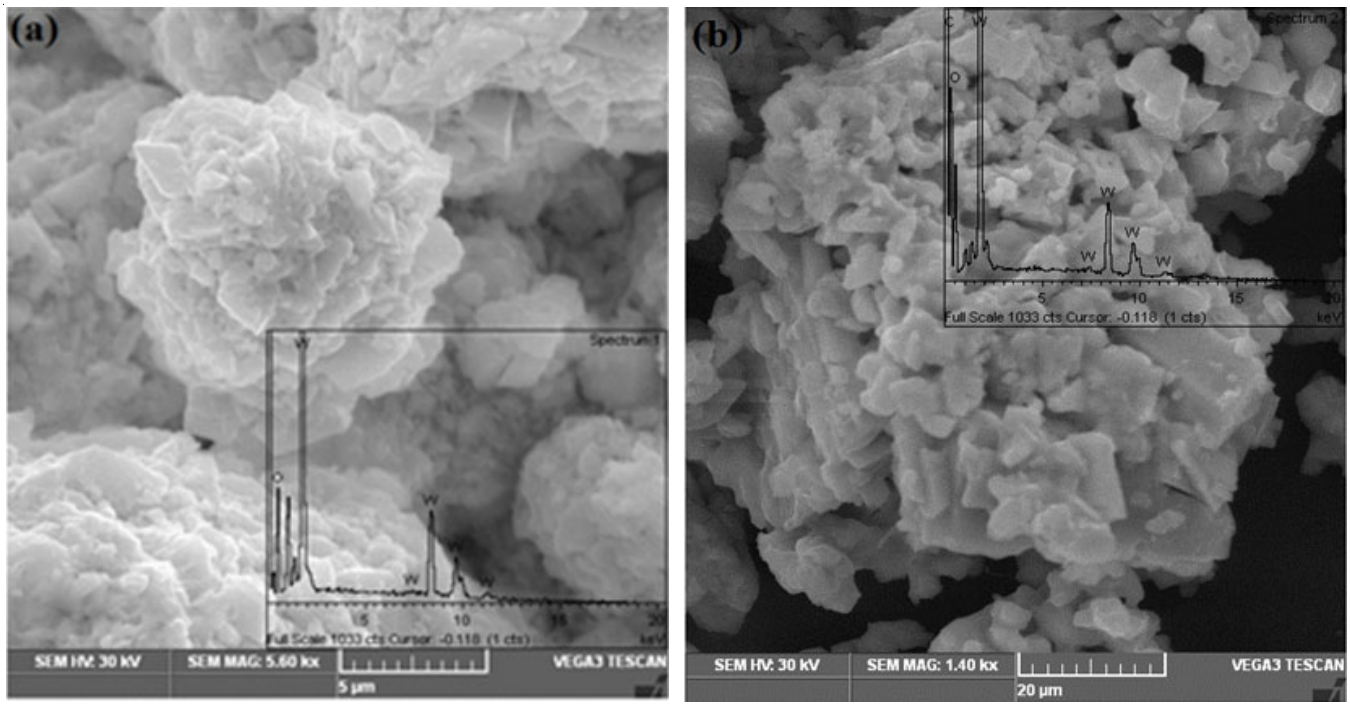

Fig. 3. SEM images of POM (a) and β-CD-POM (b)

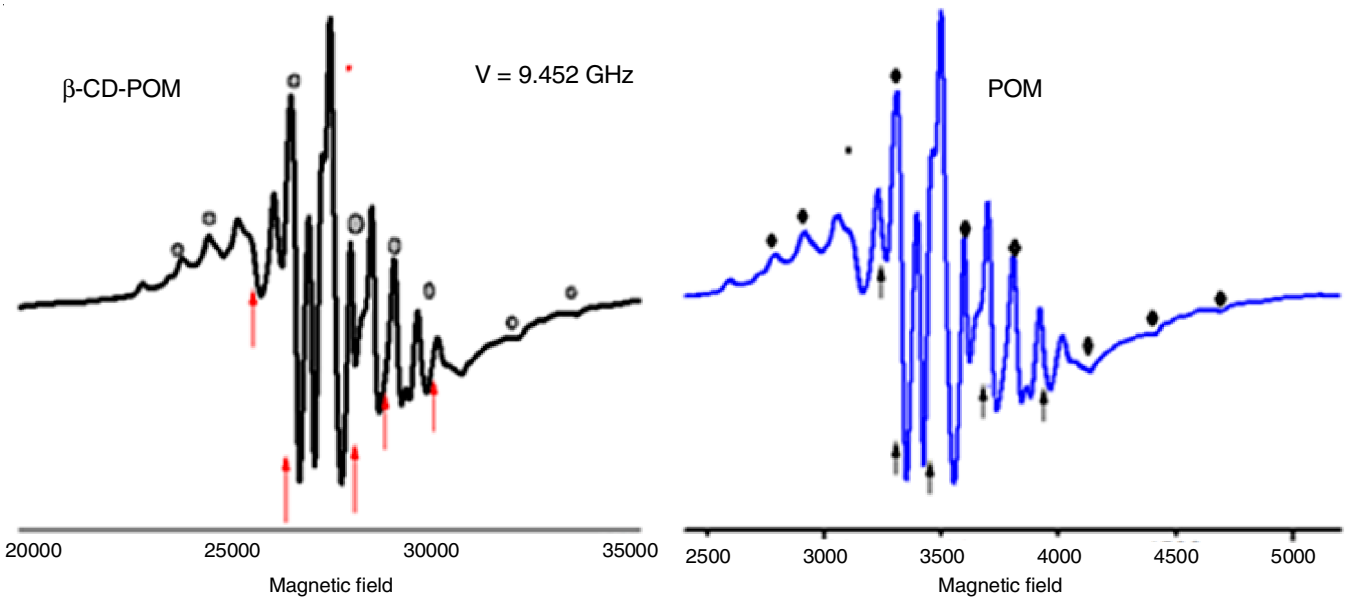

Fig. 4. EPR spectral data of POM and β-CD-POM

TABLE-3
EPR SPECTRA DATA OF POM AND β-CD-POM

Samples	g value	Reference
POM	1.90	This work
	1.94	[Ref. 28]
β-CD-POM	1.98	This work
	1.94	[Ref. 28]

Anticancer activity

Cytotoxicity assay: The effectiveness of MTT assay, at various concentrations of (3.12-100 μL/mL) was tested for its viability on cancer cell lines. The inducing apoptosis in A549 cells for the β-CD-POM was observed using direct microscopic observations of drug-treated images of cell lines by an inverted biological microscope. The cytotoxicity assay of apoptosis of cancer cell death increases as the concentrations of the cell lines increases (3.12-100 μL/mL). The untreated cell lines show no obvious signs of cell death whereas, at 3.12 μL/mL the percent of apoptosis (45.37 %) caused by β-CD-POM was slight than that caused by blank treatment. In 6.25, 12.5, 25, 50 and 100 μL/mL which shows increases the apoptosis of cell death 41.49, 35.43, 34.19. 32. 93 and 16.30 % in the cell lines MTT assay of A549 (lung cancer) (Table-4). The IC_{50} value of the A549 (lung cancer) cell lines is 1.933. This result shows the encapsulation of the drug delivery through the prepared sample β-CD-POM has high apoptosis toward the cancer cell rather from the normal cell.

Conclusion

In summary, β-CD-POM complex are synthesized and characterized using spectral techniques like IR, EPR and Impendence analyzer. The spectral data of hybrid system shows an enhancing and quenching of sharp peak is may be due to the interaction of host-guest complex. A SEM image shows a unique self-assembled morphology of flower shaped and rectangular block with size of micro meter. The X-band EPR spectral data shows the 8 lines of hyperfine structure of the presence of V^+ ions in the POM and β-CD-POM complex. The anticancer activity studies show the promising viability of the β-CD-POM against the cancer cell line of A549 (lung cancer).

ACKNOWLEDGEMENTS

The financial support from the Don Bosco Research Grant, Sacred Heart College, Tirupattur-635 601 is greatly appreciated.

CONFLICT OF INTEREST

The authors declare that there is no conflict of interests regarding the publication of this article.

TABLE-4
ANTICANCER ACTIVITY OF β-CD-POM

Sample	MTT Assay (A549 cell line): Concentration (μg)							
	Blank	Untreated	3.12	6.12	12.5	25	50	100
Reading 1	0.018	1.17	0.547	0.5	0.421	0.408	0.376	0.173
Reading 2	0.018	1.11	0.526	0.502	0.416	0.402	0.399	0.217
Reading 3	0.015	1.169	0.52	0.459	0.418	0.403	0.395	0.215
Mean	0.017	1.149	0.531	0.487	0.418	0.404	0.39	0.201
S.D.		0.0343	0.01417	0.02426	0.00251	0.0032	0.0122	0.0248
Viability (%)		100	45.379	41.494	35.432	34.196	32.93	16.303

IC_{50} value = 1.933

REFERENCES

1. H. Cao, C. Li, W. Qi, X. Meng, R. Tian, Y. Qi, W. Yang and J. Li, *PLoS One*, **12**, e0181018 (2017); https://doi.org/10.1371/journal.pone.0181018.
2. X. Wu, M.T. Trinh, D. Niesner, H. Zhu, Z. Norman, J.S. Owen, O. Yaffe, B.J. Kudisch and X.-Y. Zhu, *J. Am. Chem. Soc.*, **137**, 2089 (2015); https://doi.org/10.1021/ja512833n.
3. L. Chen, W.-L. Chen, X.-L. Wang, Y.-G. Li, Z.-M. Su and E.-B. Wang, *Chem. Soc. Rev.*, **48**, 260 (2019); https://doi.org/10.1039/C8CS00559A.
4. H. Li, P. Gong, J. Jiang, Y. Li, J. Pang, L. Chen and J. Zhao, *Dalton Trans.*, **48**, 3730 (2019); https://doi.org/10.1039/C9DT00312F.
5. S.L. Van Rompuy and T.N. Parac-Vogt, *Curr. Opin. Biotechnol.*, **58C**, 92 (2019); https://doi.org/10.1016/j.copbio.2018.11.013.
6. R. Meenakshi, K. Shakeela, S.K. Rani and G.R. Rao, *Catal. Lett.*, **148**, 246 (2018); https://doi.org/10.1007/s10562-017-2214-2.
7. T. Wei, M. Zhang, P. Wu, Y.-J. Tang, S.-L. Li, F.-C. Shen, X.-L. Wang, X.-P. Zhou and Y.-Q. Lan, *Nano Energy*, **34**, 205 (2017); https://doi.org/10.1016/j.nanoen.2017.02.028.
8. S. Xu, L. You, P. Zhang, Y. Zhang, J. Guo and C. Wang, *Chem. Commun.*, **49**, 2427 (2013); https://doi.org/10.1039/c3cc37977a.
9. W. Dong, F. Yao, Y.-G. Chen and Q. Tang, *J. Incl. Phenom. Macrocycl. Chem.*, **78**, 397 (2014); https://doi.org/10.1007/s10847-013-0310-5.
10. M.T. Pope Heteropoly and Isopoly Oxometalates, Springer-Verleg: Berlin Heidelberg (1983).
11. H. Danafar and B. Yadollahi, *J. Catal. Comm.*, **10**, 842 (2009); https://doi.org/10.1016/j.catcom.2008.12.015.
12. Y.-X. Ma, W.-J. Shao, W. Sun, Y.-L. Kou, X. Li and H.-P. Yang, *Appl. Surf. Sci.*, **459**, 544 (2018); https://doi.org/10.1016/j.apsusc.2018.08.025.
13. A.-M. Resmerita, M. Asandulesa, G. Bulai and A. Farcas, *Eur. Polym. J.*, **114**, 39 (2019); https://doi.org/10.1016/j.eurpolymj.2019.02.015.
14. G. Izzet, M. Menand, B. Matt, S. Renaudineau, L.-M. Chamoreau, M. Sollogoub and A. Proust, *Angew. Chem. Int. Ed.*, **51**, 487 (2012); https://doi.org/10.1002/anie.201106727.
15. J.E. Molinari, L. Nakka, T. Kim and I.E. Wachs, *ACS Catal.*, **1**, 1536 (2011); https://doi.org/10.1021/cs2001362.
16. C. Yang and Y. Inoue, *Chem. Soc. Rev.*, **43**, 4123 (2014); https://doi.org/10.1039/C3CS60339C.
17. K. Watanabe, H. Kitagishi and K. Kano, *Angew. Chem. Int. Ed.*, **52**, 6894 (2013); https://doi.org/10.1002/anie.201302470.
18. S. Sengupta and A. Kulkarni, *ACS Nano*, **7**, 2878 (2013); https://doi.org/10.1021/nn4015399.
19. H. Li, F. Jiang, G. Zhang, B. Li and L. Wu, *Dalton Trans.*, **48**, 5168 (2019); https://doi.org/10.1039/C8DT05146A.
20. H. Li, F. Jiang, G. Zhang, B. Li and L. Wu, *Dalton Trans.*, **48**, 3509 (2019); https://doi.org/10.1039/C9DT90056J.
21. M.A. Moussawi, N. Leclerc-Laronze, S. Floquet, P.A. Abramov, M.N. Sokolov, S. Cordier, A. Ponchel, E. Monflier, H. Bricout, D. Landy, M. Haouas, J. Marrot and E. Cadot, *J. Am. Chem. Soc.*, **139**, 12793 (2017); https://doi.org/10.1021/jacs.7b07317.
22. K.P. Sambasevam, S. Mohamad, N.M. Sarih and N.A. Ismail, *Int. J. Mol. Sci.*, **14**, 3671 (2013); https://doi.org/10.3390/ijms14023671.
23. B. Tang, Z. Chen, N. Zhang, J. Zhang and Y. Wang, *Talanta*, **68**, 575 (2006); https://doi.org/10.1016/j.talanta.2005.04.070.
24. H. Hamdi, R. Abderrahim and F. Meganem, *Spectrochim. Acta A Mol. Biomol. Spectrosc.*, **75**, 32 (2010); https://doi.org/10.1016/j.saa.2009.09.018.
25. R. Murugesan, T. Jeyabalan, P. Sami and A Shunmugasundaram, *Proc. Indian Acad. Sci. Chem. Sci.*, **110**, 7 (1998); https://doi.org/10.1007/BF02871905.
26. H.M. Dardeer, A.A. El-sisi, A.A. Emam and M. Nora Hilal, *Int. J. Textile Sci.*, **6**, 79 (2017).
27. A. Bocanegra-Diaz, N.D.S. Mohallem and R.D. Sinisterra, *J. Braz. Chem. Soc.*, **14**, 936 (2003); https://doi.org/10.1590/S0103-50532003000600011.
28. I. Kaminker, H. Goldberg, R. Neumann and D. Goldfarb, *Chem. Eur. J.*, **16**, 10014 (2010); https://doi.org/10.1002/chem.201000944.